Numerical optimisation of laser assisted friction stir welding of structural steel

Bilal Ahmad*, Alexander Galloway, Athanasios Toumpis

Department of Mechanical & Aerospace Engineering, University of Strathclyde, James Weir Building, 75 Montrose Street, Glasgow G1 1XJ, United Kingdom

* Corresponding author. Tel.: +44 (0) 141 574 5076,

e-mail address: bilal.ahmad@strath.ac.uk

Abstract

Significant progress has been made on the implementation of friction stir welding (FSW) in the industry for aluminium alloys. However, steel FSW and other high temperature alloys is still the subject of considerable research, mainly because of the short life and high cost of the FSW tool. Different auxiliary energies have been considered as a means of optimising the FSW process and reducing the forces on the tool during the plunge and traverse stages, but numerical studies on steel are particularly limited. Building on the state-of-art, laser assisted steel FSW has been numerically developed and analysed as a viable process amendment. Laser assisted FSW increased the traverse speed up to 1500 mm/min, significantly higher than conventional steel FSW. The application of laser assistance with a distance of 20 mm from the rotating tool reduced the reaction force on the tool probe tip up to 55% as compared to standard FSW.

Keywords: laser assisted friction stir welding; finite element modelling; coupled Eulerian Lagrangian; DH36; flash formation; temperature distribution

1. Introduction

Friction stir welding (FSW) is recognised as one of the most energy efficient, environmental friendly and versatile welding process [1]. Considerable research has been carried out on FSW of low melting temperature materials [2], therefore, FSW has marked its way to the joining applications for Aluminium and other alloys in industries such as shipbuilding, aerospace and automotive [3]. Investigation on the FSW prospects for high strength alloys such as steel is being conducted since last decade [4]. Various researches have demonstrated remarkable results for steel FSW [5–9].

Recently, the use of supplementary heat sources in parallel with FSW has proven to be an attractive solution to obtaining the optimised process parameters of FSW along with the reduced reaction forces on the tool [10]. The additional heat source softens the material prior to the welding process and this has the beneficial effect of reducing the stresses experienced by the tool. Various researchers [1,11–14] have used different types of assisted heat sources to analyse the behavior of the entire process. Shi et al. [11] investigated the FSW process on Aluminium by inputting ultrasonic vibrations to the workpiece. It was found that the tool torque was reduced by about 10 percent with preheating and the use of acoustic softening of the material [11]. Research by Potluri et al. [1] demonstrated the feasibility of using electric heating in the friction stir welding process on Aluminium. A large amount of current was passed

through the workpiece to generate a temperature rise along with the direct material softening [1]. The traverse force was decreased up to 59% on average as compared to the conventional friction stir welding process [1]. Another type of auxiliary heating is induction heating in which a varying electromagnetic field is setup around an electrically conductive workpiece. The workpiece is then heated by the electric current flow [15]. Alvarez et al. [13,16] performed FSW along with the induction heating of super duplex stainless steel. A decreased plunge force by 30% was observed, which extended the tool life due to the assisted induction heating [16].

A relatively simpler, yet advanced, version of the conventional FSW is the laser assisted FSW (LAFSW), which is the most extensive modification applied to the FSW process to date [12,16–20]. The experimental setup of LAFSW incorporates the FSW machine accompanied by a laser heat source. Since the maximum stresses on the tool mainly occur in the plunge stage [10], an area of workpiece, where the tool is to be plunged, is heated by a laser before the plunge stage. This helps in significantly softening the material. After the tool is in the traverse stage, the laser keeps on preheating the workpiece before the tool passes from that area. This minimises the reaction forces on the tool, which in turns helps to extend the life of the tool [10]. Figure 1 shows the schematic of LAFSW during the traverse stage.

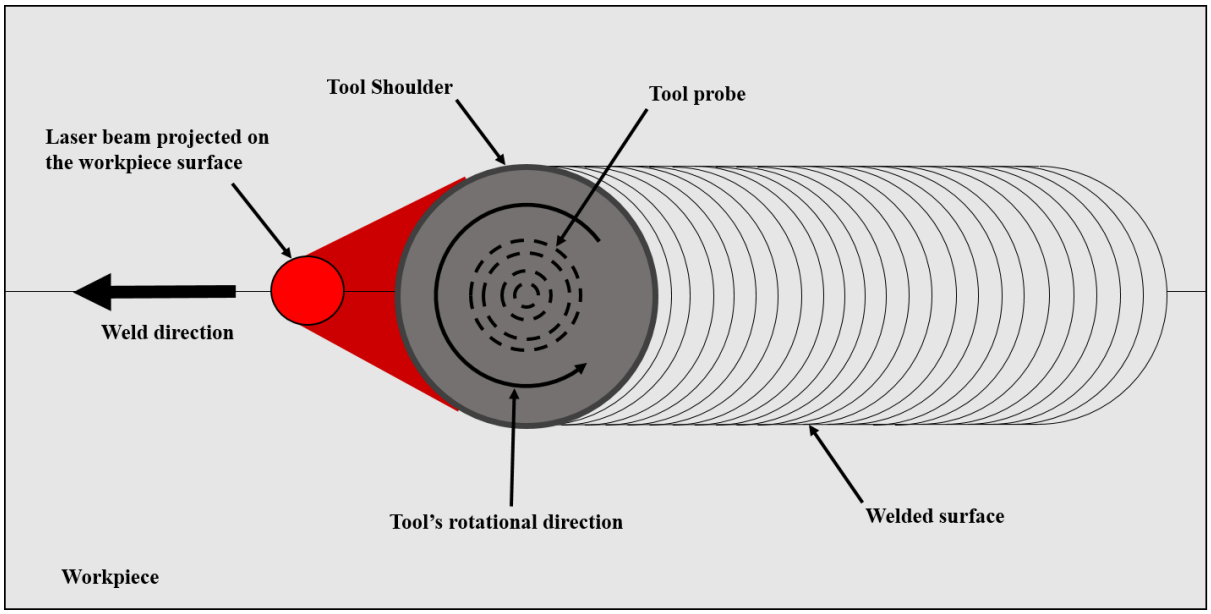

Figure 1. Schematic of LAFSW during the traverse stage.

Various experimental and modelling studies have been undertaken for LAFSW of Aluminium and other low melting temperature alloys. Casavola et al. [12] made an experimental set up for LAFSW of Aluminium 5754 and performed various tests by altering the laser power and

distance between the laser and the FSW tool. It was concluded that a closer laser distance with the FSW tool was more suitable to produce a strong preheating effect on the workpiece than a far distance irrespective of the laser power [12]. To reduce the welding forces on the FSW tool, a study was conducted by the application of laser preheating on friction stir lap welding [21]. It was found that increasing the average weld temperature and the size of the heat affected zone is not always desirable for the laser heat assistance in FSW due to the increased power consumption [21].

Limited research has been published on LAFSW of steel and other high melting temperature alloys. To optimise the process parameters, Sun et al. [18] successfully obtained an increased traverse speed (up to 800 mm/min) when joining S45C steel plates through LAFSW. The effects of offsetting the heat source from the weld centerline were observed [18]. It was observed that the total heat input can be maximized by focusing the laser beam on the retreating side as compared to the advancing side [18]. Alvarez et al. [16] welded marine steel plates by using laser preheating technique. The metal softening due to the laser heating resulted in 33% and 40% reduction in the downward forces on the tool during the plunge and traverse stages, respectively [16].

Numerical modelling is a resourceful technique as it allows the user to develop an insight of the FSW process in a cost effective manner [22], which are not readily possible through the experimental procedures. Numerical modelling of FSW has enabled to analyse the process much better than before. Daftardar [23] developed a thermal model of LAFSW in Fluent based on the FSW experiments by Zhu et al. [24]. The study demonstrated that less work is required by the tool when the preheating source is positioned in advance of the FSW tool [23]. To analyse the LAFSW of dissimilar metals, Ti-6Al-4V with stainless steel AISI 304L, Sundqvist et al. [25] developed a thermal pseudo mechanical model, which computed heat generation from the material's yield stress. A laser heat power of 600 W was applied through Nd: YAG-laser beam [25]. The laser preheating significantly reduced the forces on the tool probe and shoulder, and dropped the FSW heat generation [25].

Recently, the use of the Coupled Eulerian Lagrangian (CEL) approach has demonstrated outstanding results for modelling FSW as it can assess large deformation and strain rates [26]. Temperature distribution, reaction forces, formation of flash on the workpiece surface and material flow are some of the important results normally obtained by using this approach.

The present study presents a thermomechanical model of LAFSW of shipbuilding graded steel DH36 with the temperature dependent material properties. Use of both tool and workpiece as solid bodies improved the accuracy and similarity between numerical and experimental results. Experimental laser data [18] has been applied to provide a realistic comparison between with and without heat assisted FSW, the latter one being thoroughly discussed and validated in a previous study [26]. Temperature distribution and material flow in the workpiece along with the reaction forces on the tool have been discussed in this study. A suitable distance between moving heat source and the tool during the traverse stage has been established to minimise the reaction forces on the tool. Since a maximum traverse speed of 500 mm/min has been achieved on FSW of steel [4], LAFSW process has been simulated to maximise the existing traverse speed.

2. Methodology

2.1. Model description

A three dimensional finite element model has been produced in the finite element modelling FEM software Abaqus/Explicit. Temperature dependent material properties allowed the model to calculate the thermal and structural results, simultaneously. The CEL approach thoroughly described in the previous research [26], has been applied in the current model which enhanced the ability to measure large deformations in the model. The workpiece and the tool have been modelled as an Eulerian and Lagrangian body, respectively. The Eulerian body consisted of two regions, 'full' and 'void' [26]. The DH36 material properties were initially assigned to the full region, which is the workpiece in the present model. The purpose of the void region was to calculate and display the flash on the surface of the workpiece during the process.

LAFSW uses an additional heating source to consecutively preheat the material before and during the FSW process. In addition to the conventional stages of FSW, a heating stage is present prior to the tool plunging into the workpiece as shown in Figure 2. The total heat 'Q' generated during both FSW and LAFSW processes can be shown in Eq. 1 and 2, respectively.

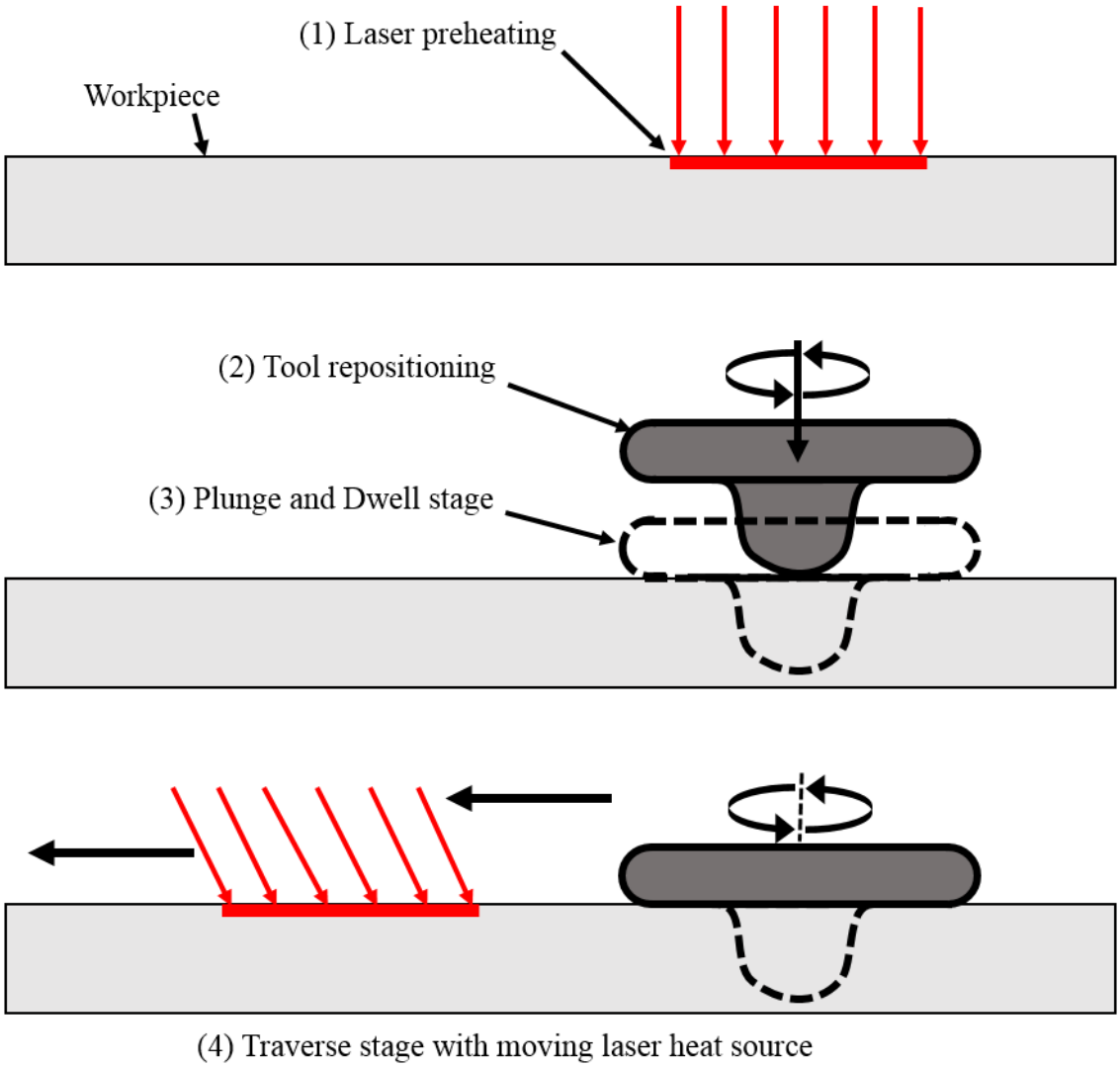

Figure 2. Systematic demonstration of LAFSW stages (side view, not to scale).

Initially, the laser heats a concentrated surface on the workpiece for 5 seconds, following which the tool immediately starts to plunge and then dwell. The preheating time has been selected so that sufficient heat is provided to the workpiece. In the traverse stage, the laser heating is applied on the workpiece through a moving heat source, as shown in Figure 2. The distance between the moving laser source and the tool is kept constant by maintaining the speeds of both the tool and the laser source. This way, the workpiece is preheated uniformly before the welding occurs. The temperature drop between the preheating and plunge stage is negligible, as the tool would take approx. 2-3 seconds for relocation to the welding position. For this reason, the tool is already placed on the plunge position in the current model to reduce the computational time.

$$Q_{FSW} = Q_{\ Friction\ between\ tool\ and\ workpiece} + Q_{Material\ deformation} \quad (1)$$

$$Q_{LAFSW} = Q_{FSW} + Q_{Laser} \quad (2)$$

$$Q_{Laser} = Initial\ preheating + Heating\ during\ the\ traverse\ stage \quad (3)$$

In LAFSW, three factors greatly influence the process; laser power, heat source diameter and the distance between the heat source and the tool. The laser power model MW 2000 YAG laser generator has been taken from the experimental setup in a previous research [18]. As concluded by Able et al. [21], increasing the average weld temperature and the size of HAZ not only affects the microstructure of the workpiece but also increases the overall power consumption. Therefore, a maximum heat of 500 W was applied for all models. Since FSW is a very localised process, the diameter of the heat source was kept small so that only workpiece surface area near the tool probe could be preheated.

2.2. Model geometry

All geometrical dimensions have been kept the same for both FSW and LAFSW models. The tool consists of a probe and shoulder. A simplified tool has been used by ignoring the spiral threads on the probe and the shoulder, thereby reducing the computational time. The thickness of the workpiece modelled in this study is 8 mm whereas the length and width have been taken as 100 mm and 60 mm, respectively. Figure 3 shows the simplified dimensions used for the tool and the workpiece.

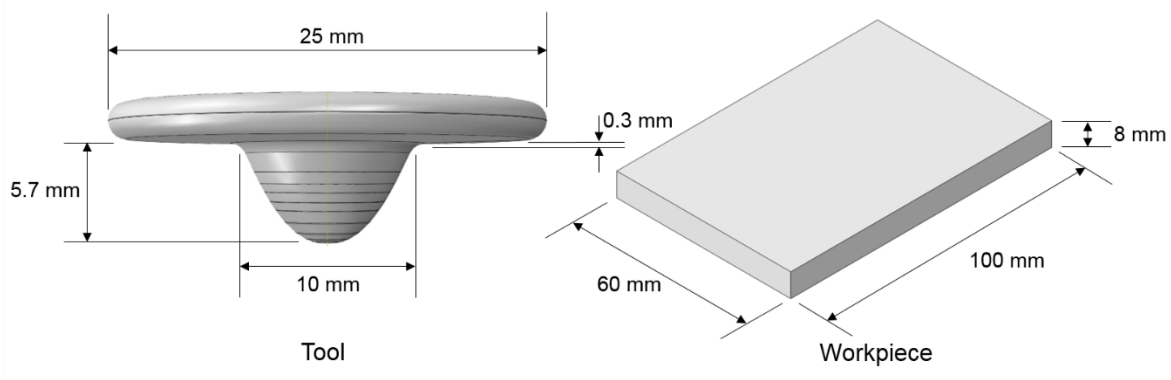

Figure 3. Geometrical dimensions of the simplified tool and the workpiece [26].

2.3. Material properties

Low alloy steel grade DH36 has been used as the workpiece for its extended usage in the shipbuilding [27]. Material properties such as thermal conductivity, specific heat and coefficient of thermal expansion have been used as temperature dependent and acquired through experimental setup from the work carried out by Micallef et al. [28]. For modelling purposes, the yield stress $\bar{\sigma}$ of DH36 steel depends on the extent of work hardening, and can be expressed as [29]:

$$\bar{\sigma} = \bar{\sigma}(\bar{\varepsilon}^{pl}, \dot{\varepsilon}^{pl}, \theta) \quad (4)$$

Where $\bar{\varepsilon}^{pl}$ is the equivalent plastic strain, $\dot{\varepsilon}^{pl}$ is the inelastic strain rate and θ is the temperature. Temperature dependent strain and strain rates from Toumpis et al [5] have been used as they accurately determined the material flow in the workpiece. Since density negligibly changed with changing temperature, it was kept as constant. The pcBN material properties were used for the tool in all LAFSW models. The thermal conductivity, specific capacity and density data for the pcBN tool has been taken from previous publications [26,30].

2.4. Process parameters

Since the aim of the current study is to consider the potential advantages of using a supplementary laser heat source, a diverse range of process parameters have been selected and modelled to compare different heat source distances. Three laser heat source distances from the tool have been modelled and discussed so that reaction forces on the tool could be minimised. The position control method was applied in the models to achieve accurate tool probe depth. Table 1 shows the process parameters for all the models discussed in the present study.

Table 1. Process parameter specifications for models to determine the suitable heat source distance from the tool.

Model name	Plunge	Dwell	Traverse

	Tool rotational speed (rpm)	Tool feed rate in downward direction (mm/min)	Tool rotational speed (rpm)	Rotating speed (rpm)	Tool traverse and laser speed (mm/min)	Distance between moving laser and tool (mm)
FSW-1[26]*	800	100	700	700	500	-
LAFSW-1	800	100	700	700	500	20
LAFSW-2	800	100	700	700	500	30
LAFSW-3	800	100	700	700	500	40

Model with * does not includes the laser source.

The model FSW – 1 has been validated through experimental data and thoroughly discussed in a previous research [26]. This has been set as a benchmark for modelling LAFSW and obtaining an appropriate heat source distance so that process parameters could be maximised. From LAFSW – 1 to 3, the weld speeds are kept constant to accurately analyse the effect of changing the distance between the moving laser heat source and the tool during the traverse stage.

2.5. Initial and boundary conditions

Initial and boundary conditions were applied to replicate real life conditions. All model settings were replicated from the model FSW – 1, also referred as the fast weld model in the previous research [26]. The entire workpiece was assigned a fixed initial temperature of 25^{o}C. A frictional coefficient of 0.3 was used to provide a feasible contact property definition between all surfaces, as discussed in previous studies [26,31]. To transfer the heat from workpiece to the surrounding, convective coefficients of 10 and 2000 W/m^{2}K were applied on the top/sides and bottom surfaces of the workpiece, respectively. The workpiece was fully constrained from the bottom surface so that no translational or rotational movement was possible on the bottom surface nodes. All of the energy generated by the frictional contact between the tool and the workpiece was converted into heat where 90% of the converted heat was assumed to be transferred into the workpiece.

A uniform mesh was specified to accurately capture all thermal and structural results. The tool was meshed with 6072 Lagrangian elements C3D8RT, whereas the workpiece was meshed with 25192 Eulerian elements EC3D8RT. Both elements are thermally coupled 8-node brick type. A gap conductance was introduced in the model to avoid any mesh irregularities between the tool and the workpiece contact surface.

In LAFSW, visualisation of the material flow is crucial as the process contains high plastic deformation [10]. In Abaqus software, tracer particles can be assigned on specified nodes of the mesh which can be later visualised in the results. Since the workpiece has been simulated as an Eulerian body, tracer particles follows the material motion irrespective of the mesh motion. Four sets of tracer particles were defined in the model so that the material flow could be thoroughly observed in all stages of the welding. The first set is located where the tool plunges and then dwells, whereas other sets were placed in the middle of the traverse stage as shown in Figure 4.

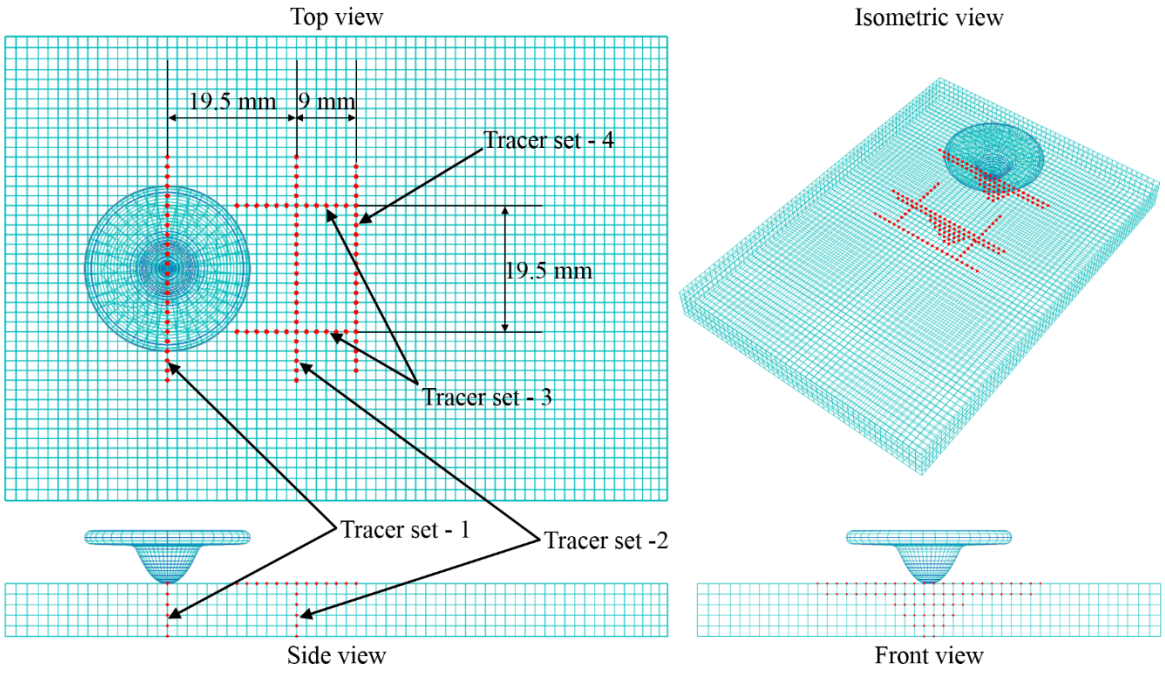

Figure 4. Initial locations of the tracer particle sets in all models.

3. Results and discussion

Several numerical models were simulated with varying auxiliary heat source distances and process parameters. However, only the notable results have been presented and discussed in the present study. As shown in Table 1, the effect of changing the heat source distance has been

compared by simple FSW, and by keeping other process parameters constant. Figure 5 shows an illustration of LAFSW weld from a side view. The duration of preheating, plunge, dwell and traverse was 5, 3.562, 4 and 10 seconds, respectively.

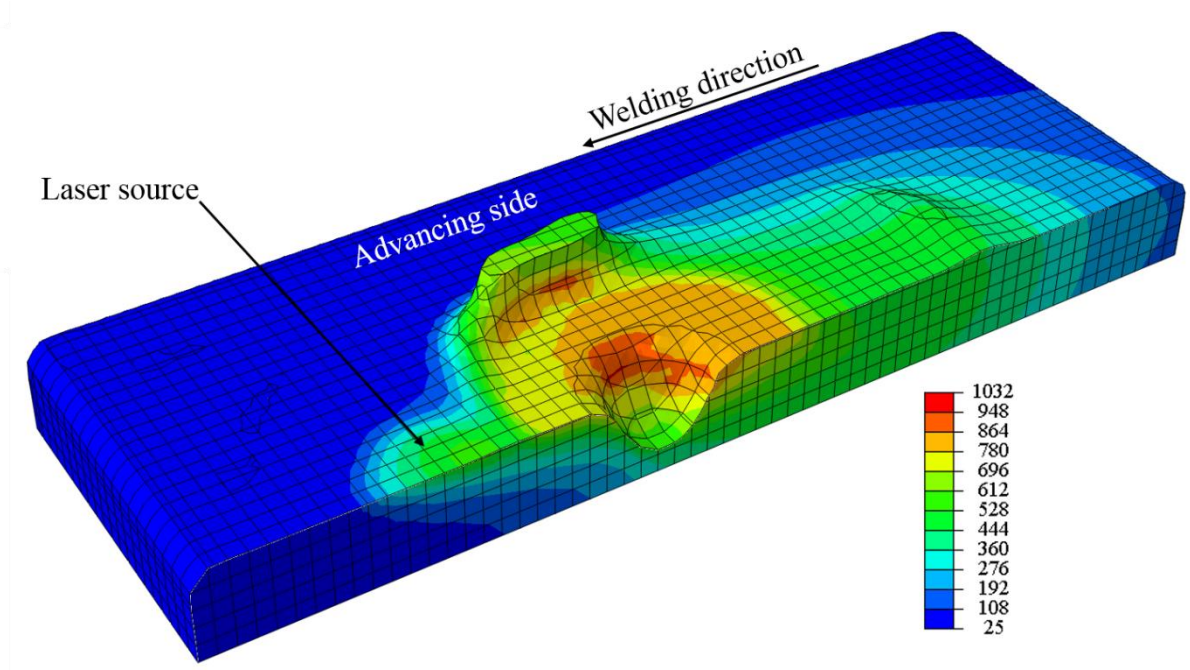

Figure 5. Lateral view of LAFSW-1 featuring the temperature distribution in ^{o}C.

3.1. Reaction forces

During both FSW and LAFSW models, the maximum stresses were measured at the lower part of the tool probe. The reaction forces on the probe tip of the tool have been calculated and presented in Figure 6. Since the tool was not in contact with the workpiece during the preheating stage, the results have been discussed only for the plunge, dwell and traverse stages. The maximum stresses occur on the tool during the plunge stage [2], also seen in Figure 6. During the first 2.7 seconds of the plunge stage, the reaction force on the probe tip increased linearly. The maximum reaction force of 120 KN is calculated right after the tool shoulder came in contact with the workpiece for the FSW-1 model. An average peak of 50 kN has been obtained for the laser assisted models during the plunge stage. The preheating of the workpiece reduced the reaction forces in LAFSW by an average difference of 65 kN compared to the conventional FSW process. This shows a reduction of approx. 55% in the reaction forces on the tool during the plunge stage with the laser assistance to the FSW process. Similar results up to 45% reduction in the downward force on the tool have been reported for Aluminium alloy 6061 in a previous research [15]. Since the preheating energy had already softened the

workpiece material, the tool probe observed a stabilised reaction force during the dwell stage. As the tool started traversing, there was a linear increase in reaction force from 7.6 to 8.8 seconds. This phenomenon occurred because the heat transferred in HAZ during preheating, plunge and dwell stages dissipated to the surroundings, hence creating a larger HAZ. After the tool no longer experienced any heat effect from the previous stages, the reaction forces were stabilised, yet minimised, due to the moving laser heating ahead of the tool.

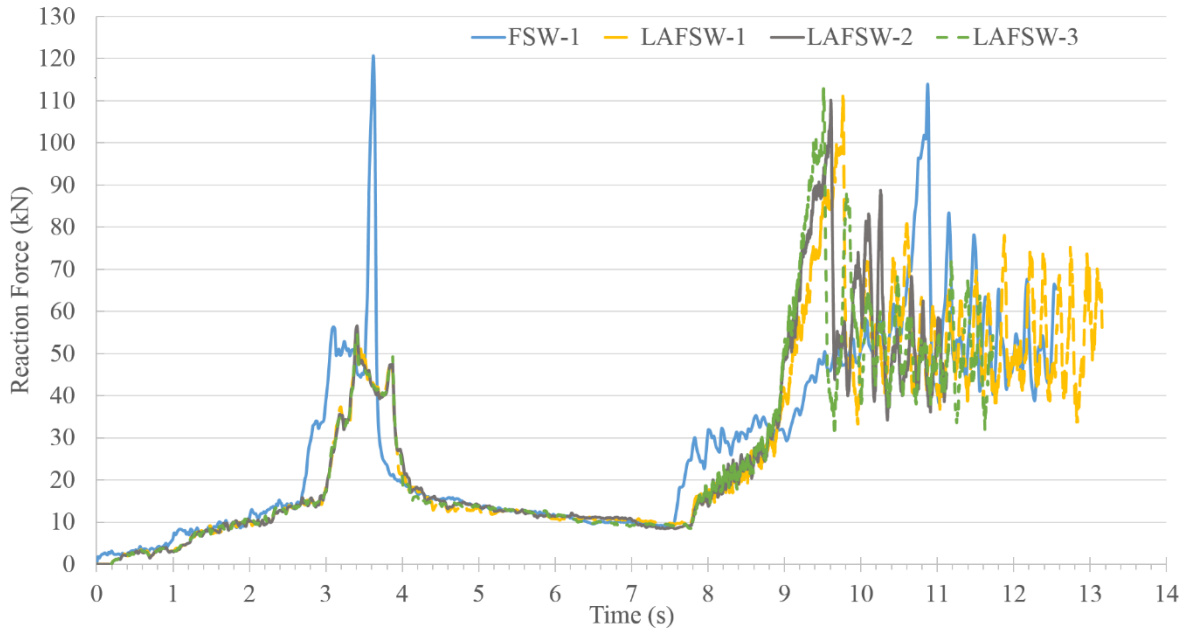

Figure 6. Reaction force comparison on the tool tip in the FSW and LAFSW models.

Among all LAFSW models discussed in this study, the least reaction force was found in the model type LAFSW-1 which comprised of a distance of 20 mm between the laser heating source and the tool rotating axis. This shows that advantages of heat assistance could be maximised by maintaining a minimum distance between the heat source and the FSW tool. The horizontal components of the reaction forces had negligible values as compared to the vertical component of the reaction force. Therefore, only the vertical component (RF2) has been presented and discussed in this work. Figure 7 represents RF2 for FSW-1 and LAFSW-1 models. It can be observed that RF2 is reduced to 55 kN in the plunge stage due to the effect of laser heating. The force components for both models follow a similar pattern in the dwell stage due to almost no laser heat influence. In the traverse stage, RF2 observed an initial linear increase as discussed previously in the Figure 6. A substantial difference between the forces of FSW and LAFSW has not been observed during the traverse stage. This is due to the fact that

the heat generated due to the laser heat source did not greatly influence the bottom surface of the workpiece.

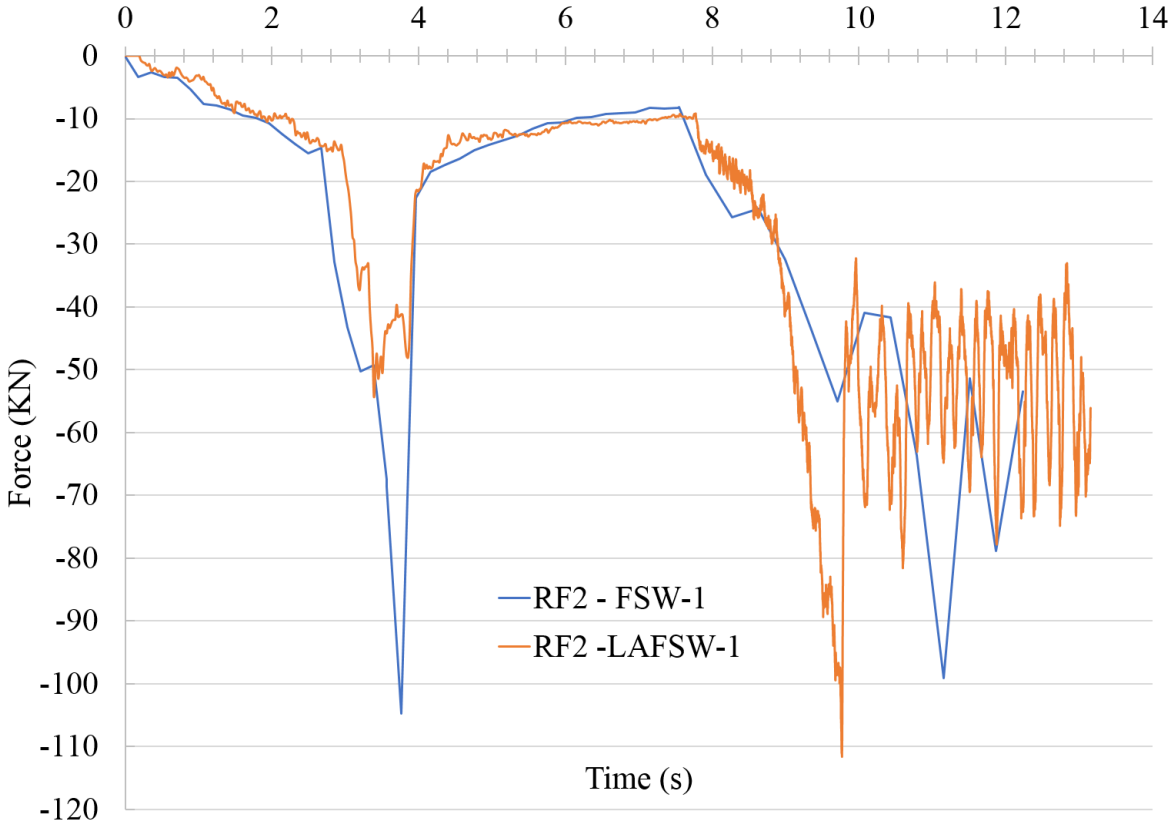

Figure 7. Reaction force components comparison for FSW-1 and LAFSW-1 models.

3.2. Temperature distribution

Figure 8 shows the temperature distribution from the top and side view for LAFSW welding configurations during the preheating stage. A peak temperature of 953 ºC was calculated in the preheating stage. Since no changes have been made in the preheating stage for all models, a temperature gradient of 224ºC is recorded at 1.6 mm from the bottom surface of the workpiece. This shows that sufficient heat could be dissipated in the expected TMAZ within 5 seconds of heating before the plunge stage.

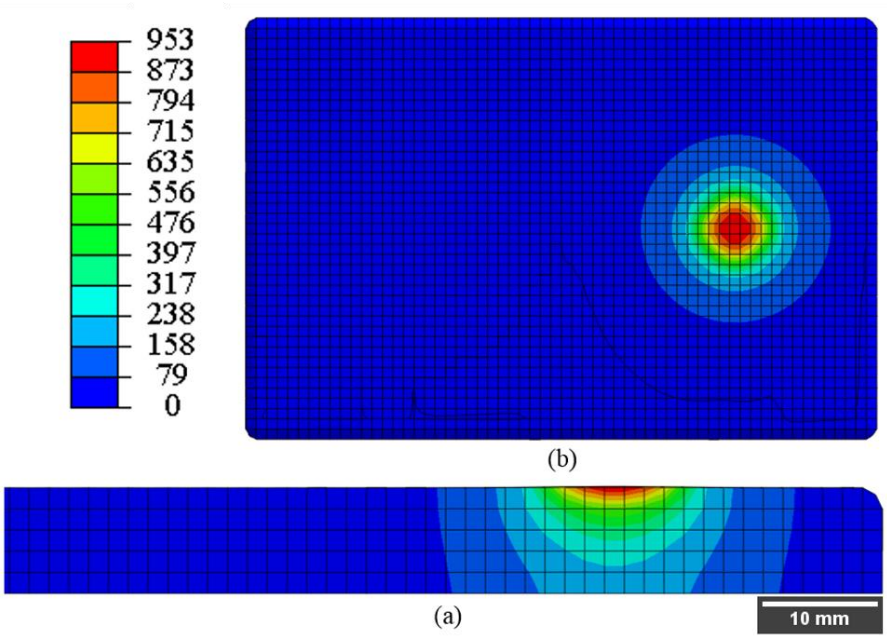

Figure 8. Temperature distribution in ^{o}C in LAFSW after the laser preheating/before the plunge stage; (a) Side view of the weld model, (b) Top view – Not set according to the scale. (Counterclockwise tool rotation).

In the dwell stage, the temperature in the TMAZ is higher in LAFSW compared to FSW (Figure 9). This is because a reasonable amount of heat was already present in the workpiece that increased the temperature in TMAZ and HAZ regions. This suggests that the total duration of dwelling stage could be reduced without even compromising the overall temperature distribution in the weld region.

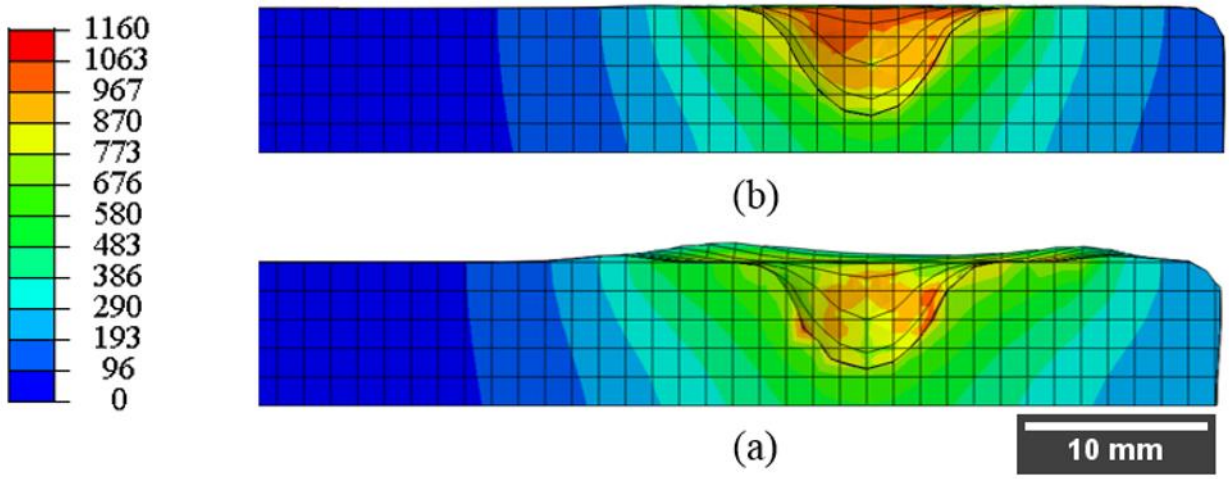

Figure 9. Temperature distribution in ^{o}C at the dwell stage; (a) Side view of the FSW-1 model, (b) side view of the LAFSW-1 model. (Counterclockwise tool rotation).

Figure 10 demonstrates isometric views of the temperature distribution for all models during the traverse stage. Models LAFSW – 1, 2 and 3, as shown in Table 1, represent the laser heat source centre at distances of 20, 30 and 40 mm from the rotating tool centre of axis, respectively. A higher temperature was observed in the advancing side (AS) of all welds as compared to the retreating side (RS). This asymmetric temperature distribution in the welding region demonstrates that the rotational direction of the tool also helps in heat flow from AS to RS.

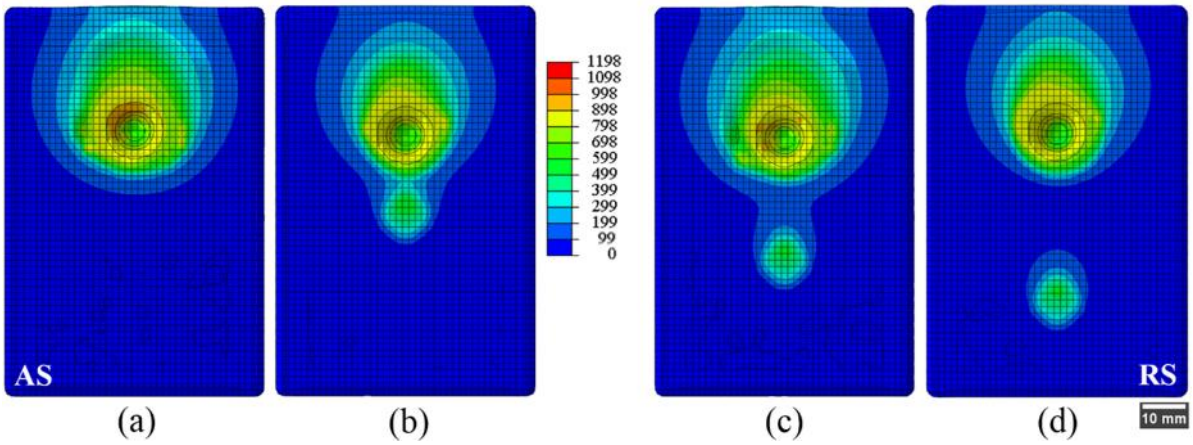

Figure 10. Temperature distribution in ^{o}C in the isometric views of; (a) FSW-1 model without laser heating, (b) LAFSW-1 model with 20 mm heat source distance, (c) LAFSW-2 model with 30 mm heat source distance, (d) LAFSW-3 model with 40 mm heat source distance. (Counterclockwise tool rotation).

The temperature contours of laser heating created an oblong effect due to the continuous movement along with the traversing tool (Figure 10). A wider temperature zone of about 900^{o}C reached near the tool shoulder in the model type LAFSW-1, which shows that the use of laser heating with a distance of 20 mm provides a possibility of least weld defects. Figure 11 demonstrates the temperature distribution in all models discussed in the Table 1, with respect to the displacement along the weld line. A comparatively higher surface temperature of 580^{o}C was recorded when the laser heating distance was set at 20 mm from the tool's centre. This also shows the potential application of using a minimum heat source distance to achieve higher temperature gradients.

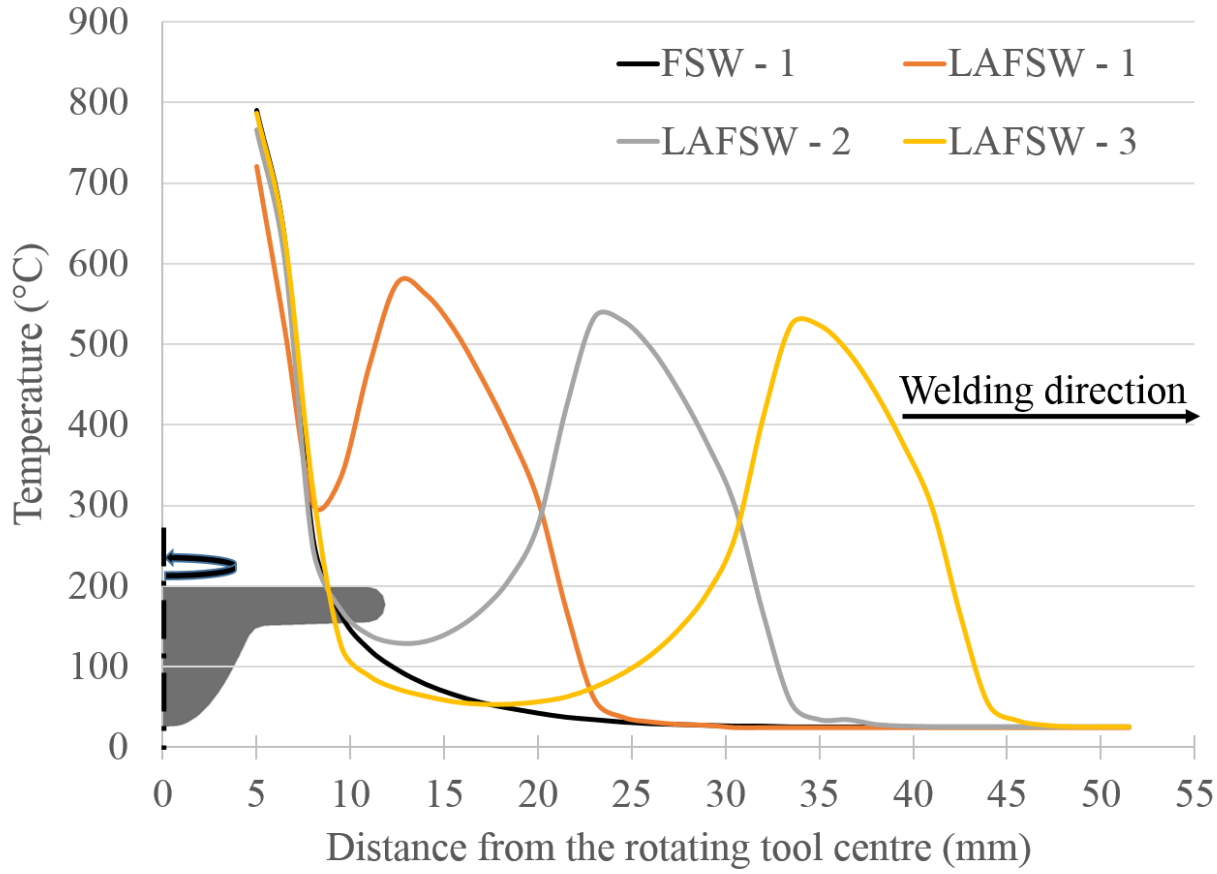

Figure 11. Surface temperature comparison for all discussed models along the welding line in front of the FSW tool.

3.3. Material flow

Visualising the material flow during and after the welding process is of great significance as it assists in the better understanding of the material deformation and the development of a defect-free weld. Numerical simulation helps in envisioning the material flow, which is not easily possible with the experimental setup. This section discusses the material movement by visualising tracer particles present in the workpiece. The initial positions for all tracer sets, shown in Figure 4, assisted in capturing the material movement in terms of mesh nodes through plunge and traverse stages of both FSW and LAFSW models. Visualising the material flow through the help of tracer particles allowed the HAZ and TMAZ regions to be identified.

Figure 12 demonstrates the positions of the tracer particles at the end of the plunge stage (t=3.652 s). During the plunge stage, the tool penetrates in the workpiece material like a drilling process. Since the region close to the tool-workpiece contact was not plasticised due to

insufficient heat generation, slight material movement was observed in the rotational direction along with the tool. As the temperature became higher in the plunge region, the tracer particles exhibiting the material flow started to swirl in the anti-clockwise direction as seen in Figure 12. It is established that the material flow is improved when preheating the workpiece than the conventional FSW.

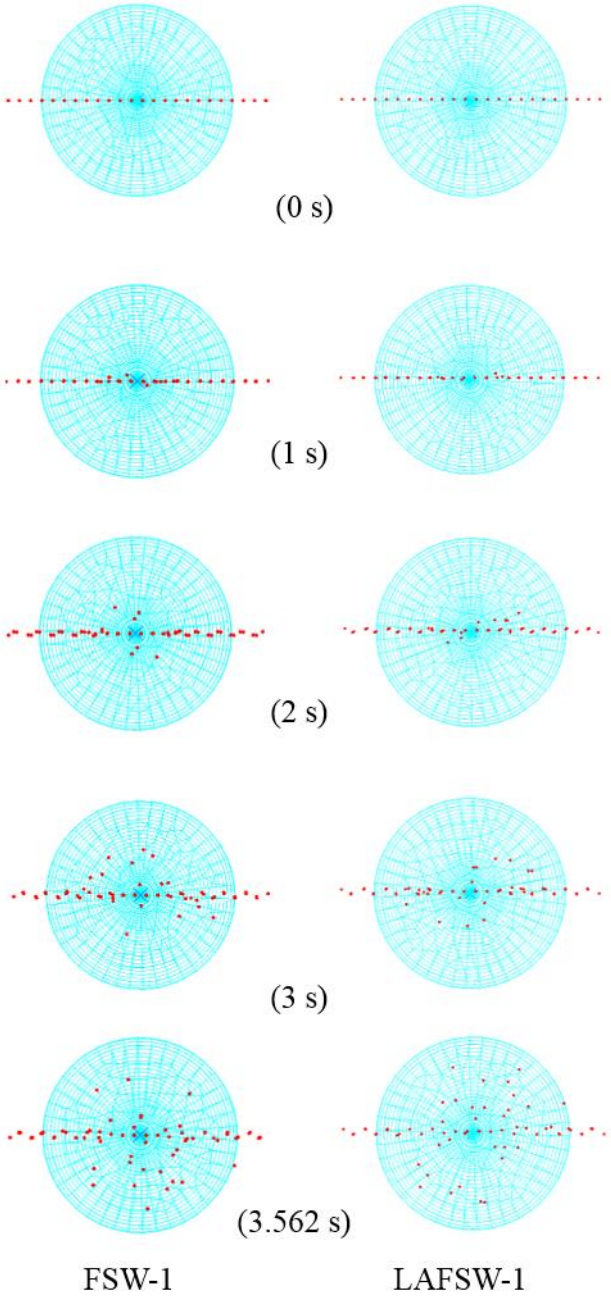

Figure 12. Material flow comparison in FSW-1 and LAFSW-1 models during the plunge stage. (Tool rotation: Counterclockwise direction).

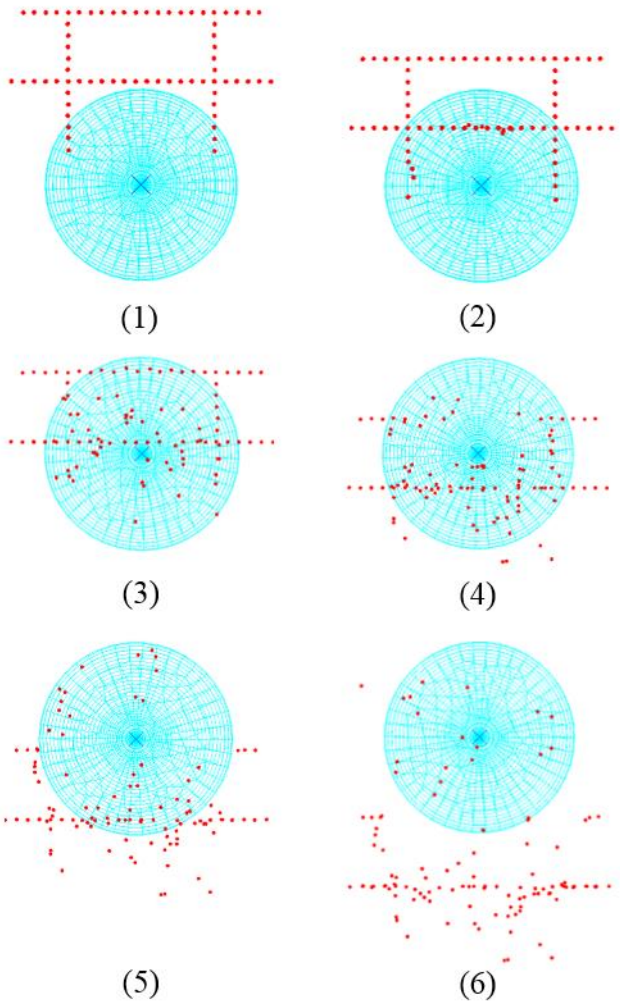

Figure 13. Material flow in the FSW-1 model during the traverse stage (1 to 6 represents periodic movement of the tool to the upward direction - Tool rotation: Counterclockwise direction).

When the tool traversed in the weld direction, the workpiece material located slightly ahead of the tool's geometry began to follow the movement of the tool, swirling from the advancing side to the retreating side. Figure 13 and 14 show the material movement through the tracer particles in FSW-1 and LAFSW-1, respectively. Once the tool moved away, some of the particles were mixed and left behind while some of them kept swirling around the moving tool (Figure 13 and 14). The tracer particles were located at the distance of 4.5 mm from the initial tool's position for FSW-1, and 10.5 mm for LAFSW-1 model. To present a better understanding for tracing material flow, a constant time step was set between all images in Figure 13 and 14. The material flow visualisation of both models depict that the addition of

laser heat source allows the workpiece material to move in the traverse stage more vigorously and distantly.

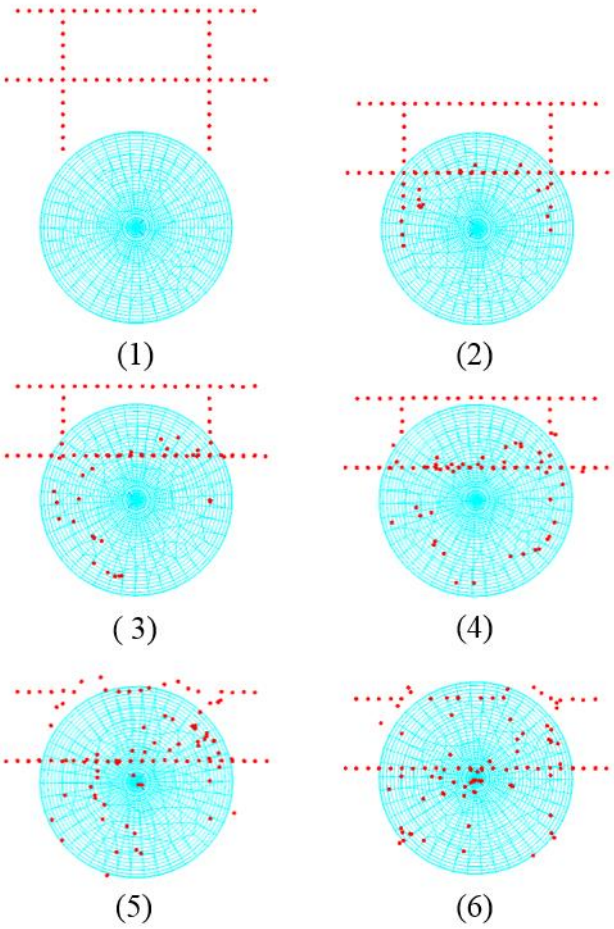

Figure 14. Material flow in the LAFSW-1 model during the traverse stage (1 to 6 represents periodic movement of the tool to the upward direction - Tool rotation: Counterclockwise direction).

3.4. Optimised LAFSW process parameters

Besides visualising the material flow during the whole process, which cannot be achieved experimentally, another significant advantage of numerical simulation of FSW/LAFSW is to guide the experimental procedures by providing optimised process parameters for excellent quality welds at high welding speeds. The temperature distribution in the workpiece (Figure 10) revealed that sufficient heat dissipated in the TMAZ and HAZ in all distances. However, Figure 6 demonstrated that the lowest reaction force was calculated with the distance of 20 mm

for all weld stages. This showed that a distance of 20 mm is appropriate when applying the laser heating with FSW as compared to other distances.

Several models with different process parameters were selected and simulated, for both FSW and LAFSW, to obtain defect-free welds with substantially increased traverse speed. Potential defects in the workpieces were analysed, and their results have been presented in the Table 2. All model results were calculated on the basis of varying the traverse and rotational speed of the tool while certain welding conditions such as backing plate, FSW tool material, clamping configuration, etc. remained constant. A fixed distance of 20 mm between moving heat source and the tool has been used for all LAFSW models, discussed in the Table 2.

Table 2. Process parameters specifications for models for the optimisation of LAFSW process.

Model name	Process Parameters		Presence of defects
	Traverse speed (mm/min)	Rotational velocity (rpm)	
FSW-1 [26]	500	700	No
FSW-2	1000	1000	Yes
LAFSW-4	700	700	No
LAFSW-5	900	700	No
LAFSW-6	1000	700	No
LAFSW-7	1200	700	Yes
LAFSW-8	1000	1500	Yes
LAFSW-9	1000	1800	No

LAFSW-10	1500	1800	No
LAFSW-11	2000	2000	Yes
FSW-3	1500	1800	Yes

Since a maximum traverse speed of 800 mm/min has been achieved by laser preheating in FSW of S45C steel [18], numerical attempts have been made in the present study to increase the traverse speed by the application of laser heating. As a consequence, no defects were observed in the conventional FSW process until the traverse speed was increased up to 1000 mm/min (Table 2). Root flaws and other surface defects appeared in the FSW-2 model. To prevent these issues, the LAFSW models were simulated with increased process parameters (LAFSW-4 to 11). It was observed that fine quality weld could be obtained up to 1500 mm/min of traverse speed by using laser heat assistance. Figure 15 shows the temperature distribution of the LAFSW model with a traverse speed of 1500 mm/mm and rotational speed of 1800 rpm.

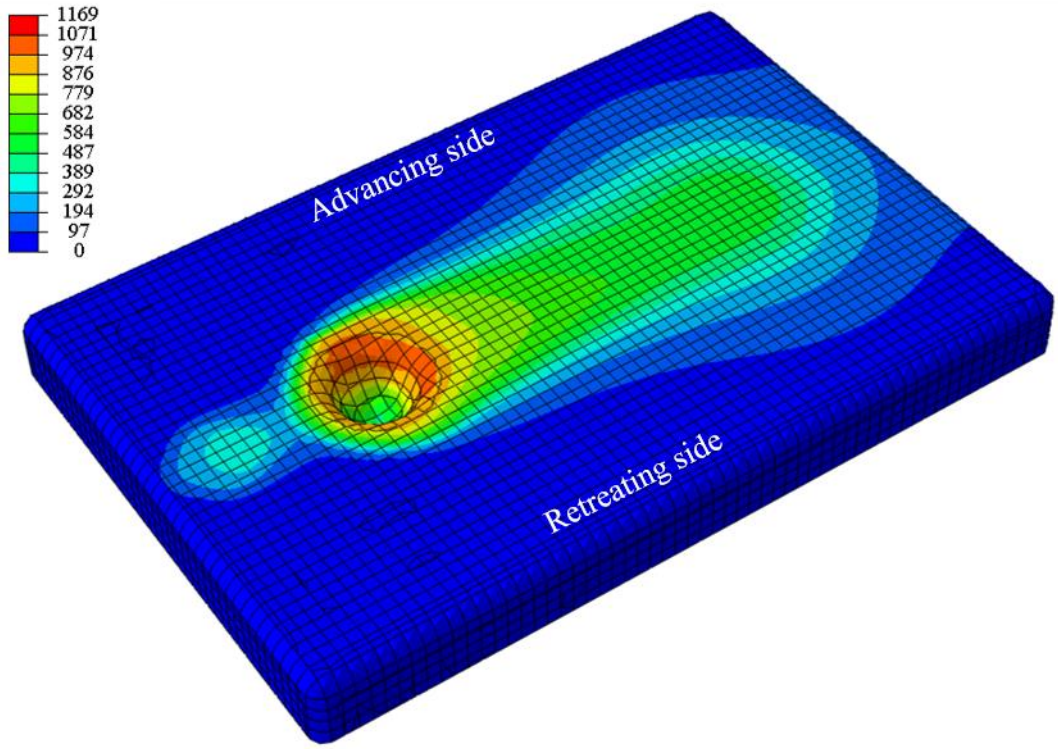

Figure 15. Temperature distribution in ^{o}C in the parametric view with increased process parameters in the LAFSW-10 model (Counterclockwise tool rotation).

To compare the results at the increased traverse speed, an FSW model was simulated without any laser heat assistance, named as FSW-3 model in Table 2. The results showed initiation of potential defects in the weld region without laser heat assistance (Figure 16). This provides further evidence on the usability of laser heating assistance at considerably higher welding speeds.

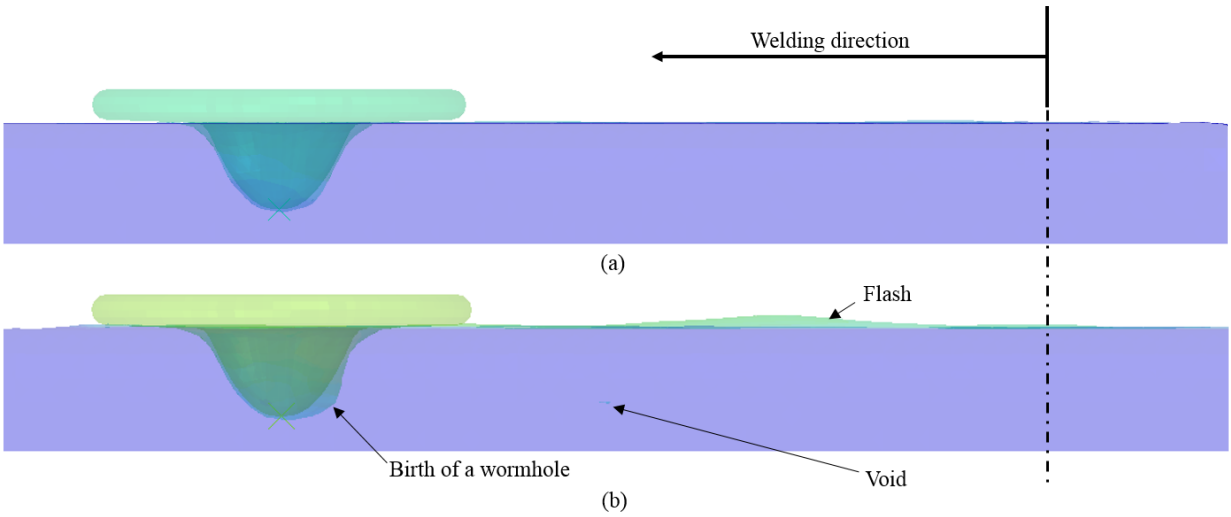

Figure 16. Visualisation of flash and weld defects from the side view in the (a) LAFSW-4 model, (b) FSW-2 model.

4. Conclusions

Fully coupled thermomechanical FSW and LAFSW models have been simulated in Abaqus/Explicit. The use of experimentally generated temperature dependent material properties for low alloy steel grade DH36 and the coupled Eulerian and Lagrangian (CEL) approach assisted in generating more accurate results than other modelling techniques used in the relevant technical literature. Experimentally applicable laser heat parameters were used as preheating and moving heat source in LAFSW. Reaction forces on the tool probe tip along with the temperature distribution and material flow in the workpiece were compared to define an appropriate distance between the tool and the moving heat source. Optimised process parameters were calculated to achieve defect-free welds and minimise reaction forces on the tool during LAFSW. It was concluded that by using LAFSW with the specified conditions, a maximum traverse speed of 1500 mm/min (with rotational speed of 1800 rpm) could be achieved without compromising the weld quality. This represents a considerable increase compared to the previously achieved welding speeds. Moreover, a distance of 20 mm between

the laser heat source and the tool presented the lowest tool reaction forces during the plunge stage, and a reasonable temperature distribution in the workpiece throughout the process. LAFSW reduced the tool reaction forces up to 55% compared to the conventional FSW. Laser heating is an efficient and convenient assisted energy in terms of providing defect-free welds and an easy fix to currently operational FSW equipment. As a result, LAFSW will increase the tool life during the plunge stage, and enhance the productivity in potential industrial applications.

Acknowledgements

Results were obtained using the EPSRC funded ARCHIE-WeSt High Performance Computer (www.archie-west.ac.uk). EPSRC grant no. EP/K000586/1.

References

[1] Potluri H, Jones JJ, Mears L. Comparison of Electrically-Assisted and Conventional Friction Stir Welding Processes by Feed Force and Torque. ASME 2013 Int. Manuf. Sci. Eng. Conf. [Internet]. 2013;V001T01A055. Available from: http://proceedings.asmedigitalcollection.asme.org/proceeding.aspx?doi=10.1115/MSEC2013-1192.

[2] Rai R, De A, Bhadeshia HKDH, et al. Review: friction stir welding tools. Sci. Technol. Weld. Join. [Internet]. 2011;16:325–342. Available from: http://www.tandfonline.com/doi/full/10.1179/1362171811Y.0000000023.

[3] Gibson BT, Lammlein DH, Prater TJ, et al. Friction stir welding: Process, automation, and control. J. Manuf. Process. [Internet]. 2014;16:56–73. Available from: http://dx.doi.org/10.1016/j.jmapro.2013.04.002.

[4] Toumpis A, Galloway A, Cater S, et al. Development of a process envelope for friction stir welding of DH36 steel - A step change. Mater. Des. [Internet]. 2014;62:64–75. Available from: http://dx.doi.org/10.1016/j.matdes.2014.04.066.

[5] Toumpis AI, Galloway AM, Arbaoui L, et al. Thermomechanical deformation behaviour of DH36 steel during friction stir welding by experimental validation and modelling. Sci. Technol. Weld. Join. [Internet]. 2014;19:653–663. Available from: http://www.tandfonline.com/doi/full/10.1179/1362171814Y.0000000239.

[6] Al-moussawi M, Smith AJ, Young A, et al. Modelling of friction stir welding of DH36 steel. Int. J. Adv. Manuf. Technol. [Internet]. 2017;92:341–360. Available from: http://link.springer.com/10.1007/s00170-017-0147-y.

[7] Polezhayeva H, Toumpis AI, Galloway AM, et al. Fatigue performance of friction stir welded marine grade steel. Int. J. Fatigue [Internet]. 2015;81:162–170. Available from: http://www.sciencedirect.com/science/article/pii/S0142112315002558.

[8] Camilleri D, Micallef D, Mollicone P. Thermal stresses and distortion developed in mild steel DH36 friction stir-welded plates: An experimental and numerical assessment. J. Therm. Stress. [Internet]. 2015;38:485–508. Available from: http://www.scopus.com/inward/record.url?eid=2-s2.0-84929464513&partnerID=40&md5=95279f825b3b8be2f78827badb5c8098.

[9] Cho JH, Boyce DE, Dawson PR. Modeling strain hardening and texture evolution in friction stir welding of stainless steel. Mater. Sci. Eng. A. 2005;398:146–163.

[10] Padhy GK, Wu CS, Gao S. Auxiliary energy assisted friction stir welding – status review. Sci. Technol. Weld. Join. [Internet]. 2015;20:1362171815Y.000. Available from: http://www.maneyonline.com/doi/abs/10.1179/1362171815Y.0000000048#.Vbm-0GV59w8.mendeley.

[11] Shi L, Wu CS, Sun Z. An integrated model for analysing the effects of ultrasonic vibration on tool torque and thermal processes in friction stir welding. Sci. Technol. Weld. Join. [Internet]. 2017;1718. Available from: https://doi.org/10.1080/13621718.2017.1399545.

[12] Casavola C, Cazzato A, Moramarco V. Thermographical Analysis of Friction Stir Welding and Laser Assisted Friction Stir Welding. XIII Youth Symp. Exp. Solid Mech. Decin, Czech Republic; 2014. p. 15–19.

[13] Álvarez AI, García M, Pena G, et al. Evaluation of an induction-assisted friction stir welding technique for super duplex stainless steels. Surf. Interface Anal. 2014;46:892–896.

[14] Santos TG, Miranda RM, Vilaca P. Friction Stir Welding assisted by electrical Joule

effect. J. Mater. Process. Technol. 2014;214:2127–2133.

[15] Sinclair PC, Longhurst WR, Cox CD, et al. Heated friction stir welding: An experimental and theoretical investigation into how preheating influences process forces. Mater. Manuf. Process. 2010;25:1283–1291.

[16] Álvarez AI, Cid V, Pena G, et al. Assisted friction stir welding of carbon steel: Use of induction and laser as preheating techniques. Frict. Stir Weld. Process. VII. 2016;117–126.

[17] Campanelli SL, Casalino G, Casavola C, et al. Analysis and comparison of friction stir welding and laser assisted friction stir welding of aluminum alloy. Materials (Basel). 2013;6:5923–5941.

[18] Sun YF, Konishi Y, Kamai M, et al. Microstructure and mechanical properties of S45C steel prepared by laser-assisted friction stir welding. Mater. Des. [Internet]. 2013;47:842–849. Available from: http://dx.doi.org/10.1016/j.matdes.2012.12.078.

[19] Chang WS, Rajesh SR, Chun CK, et al. Microstructure and Mechanical Properties of Hybrid Laser-Friction Stir Welding between AA6061-T6 Al Alloy and AZ31 Mg Alloy. J. Mater. Sci. Technol. [Internet]. 2011;27:199–204. Available from: http://dx.doi.org/10.1016/S1005-0302(11)60049-2.

[20] Song KH, Tsumura T, Nakata K. Development of Microstructure and Mechanical Properties in Laser-FSW Hybrid Welded Inconel 600. Mater. Trans. 2009;50:1832–1837.

[21] Able N, Pfefferkorn F. Laser-assisted friction stir lap welding of aluminum. ASME 2005 Summer Heat Transf. Conf. collocated with ASME 2005 Pacific Rim Tech. Conf. Exhib. Integr. Packag. MEMS, NEMS, Electron. Syst. 2005;425–429.

[22] Camilleri D, Micallef D, Arbaoui L, et al. Numerical Modelling Techniques Applicable for the Prediction of Residual Stresses and Distortion due to Mild Steel DH36 Friction Stir Welding. 4th Int. Conf. Frict. Stir Welding, FSWP2015. Spain; 2015. p. 1–5.

[23] Daftardar S. Laser Assisted Friction Stir Welding: Finite Volume Method and Metaheuristic Optimization. Louisiana State University; 2009.

[24] Zhu XK, Chao YJ. Numerical simulation of transient temperature and residual stresses in friction stir welding of 304L stainless steel. J. Mater. Process. Technol. 2004;146:263–272.

[25] Sundqvist J, Kim K, Bang H, et al. Numerical simulation of laser preheating of friction stir welding of dissimilar metals. 2017;1718. Available from: https://doi.org/10.1080/13621718.2017.1391936.

[26] Ahmad B, Galloway A, Toumpis A. Advanced numerical modelling of friction stir welded low alloy steel. J. Manuf. Process. [Internet]. 2018;34:625–636. Available from: https://doi.org/10.1016/j.jmapro.2018.07.003.

[27] Toumpis A, Galloway A, Cater S, et al. A techno-economic evaluation of friction stir welding of DH36 steel. 10th Int. Symp. Frict. Stir Weld. 2014.

[28] Micallef D, Camilleri D, Toumpis A, et al. Local heat generation and material flow in friction stir welding of mild steel assemblies. Proc. Inst. Mech. Eng. Part L J. Mater. Des. Appl. 2015;230:586–602.

[29] Simulia 6.14. Abaqus Documentation. 23.2.3 Rate-dependent yield. 2014.

[30] MegaStir. Friction Stir Welding of High Melting Temperature Materials. 2013.

[31] Ambroziak A, Winnicki M, Laska P, et al. Examination of friction coefficient in friction welding process of tubular steel elements. Arch. Metall. Mater. 2011;56:975–980.